Progress In Electromagnetics Research B, Vol. 56, 109–136, 2013

MATHEMATICAL MODELS OF ELECTRODYNAMICAL PROCESSES OF WAVE SCATTERING AND GENERATION ON CUBICALLY POLARISABLE LAYERS

Lutz Angermann[1, *] and Vasyl V. Yatsyk[2]

[1]TU Clausthal, Department of Mathematics, Erzstr. 1, Clausthal-Zellerfeld D-38678, Germany

[2]O.Ya. Usikov Institute for Radiophysics and Electronics NASU, 12 Ac. Proskura Str., Kharkiv 61085, Ukraine

Abstract—Results of a self-consistent computational analysis based on a mathematical model of resonance scattering and generation of waves on an isotropic nonmagnetic nonlinear layered dielectric structure excited by a packet of plane waves are presented, where the analysis is performed in the domain of resonance frequencies. Physically interesting properties of the nonlinear permittivities of the layers as well as their scattering and generation characteristics are obtained, for instance the characteristic dynamical behaviour of the relative Q-factor of the eigenmodes and the energy of higher harmonics generated by canalising as well as decanalising nonlinear layers. The results demonstrate the possibility to control the scattering and generating properties of a nonlinear structure by means of the excitation intensities.

1. INTRODUCTION

We investigate the problem of scattering and generation of waves on an isotropic, nonmagnetic, linearly polarised (E-polarisation), nonlinear, layered, cubically polarisable, dielectric structure, which is excited by a packet of plane waves, in the domain of resonance frequencies. We consider wave packets consisting of both a strong electromagnetic field at the excitation frequency and weak fields at multiple frequencies.

The resulting mathematical model can be represented equivalently by a system of nonlinear boundary-value problems of Sturm-Liouville type or by a system of one-dimensional nonlinear integral equations.

Received 2 September 2013, Accepted 16 October 2013, Scheduled 24 October 2013

* Corresponding author: Lutz Angermann (lutz.angermann@tu-clausthal.de).

The solution of the latter system is approximated numerically by the help of a quadrature method. The numerical algorithms of the solution of the nonlinear problems are based on iterative procedures which require the solution of a linear system in each step. The analytical continuation of these linear problems into the region of complex values of the frequency parameter allows us to switch to the investigation of spectral problems.

Some results of calculations of characteristics of the scattered field of a plane wave are presented, taking into account the third harmonic generated by nonlinear cubically polarisable layers with both negative as well as positive values of the cubic susceptibility of the medium. We show that layers with negative and positive values of the coefficient of cubic susceptibility of the nonlinear medium have fundamentally different scattering and generation properties in the domain of resonance. In the case of negative/positive values of the susceptibility, a decanalisation/canalisation of the electromagnetic field can be observed.

The paper is organized as follows: In the subsequent section, we introduce the mathematical model. Then, in Section 3, we describe the basic elements of the numerical method. The main part is formed by Section 4, where we discuss the results of numerical simulations of single-layered structures with both negative (Subsection 4.1) as well as positive (Subsection 4.2) values of the cubic susceptibility.

2. WAVE PROPAGATION IN NONLINEAR MEDIA WITH CUBIC POLARISABILITY

We consider nonlinear media which are located in the region

$$\left\{\mathbf{r} = (x, y, z)^\top \in \mathbb{R}^3 : \ |z| \leq 2\pi\delta\right\},$$

$\delta > 0$ (cf. Figure 1), such that the vector of the polarisation moment $\mathbf{P}$ can be expanded as $\mathbf{P} = \boldsymbol{\chi}^{(1)}\mathbf{E} + (\boldsymbol{\chi}^{(2)}\mathbf{E})\mathbf{E} + ((\boldsymbol{\chi}^{(3)}\mathbf{E})\mathbf{E})\mathbf{E} + \ldots$, where $\boldsymbol{\chi}^{(1)}$, $\boldsymbol{\chi}^{(2)}$, $\boldsymbol{\chi}^{(3)}$ are the media susceptibility tensors. In the case of isotropic media, the quadratic term disappears.

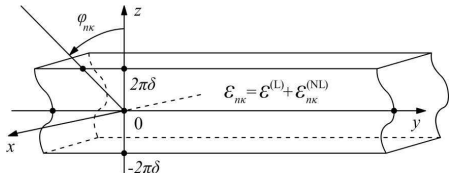

Figure 1. The nonlinear dielectric layered structure.

It is convenient to split $\mathbf{P}$ into its linear and nonlinear parts as $\mathbf{P} = \mathbf{P}^{(L)} + \mathbf{P}^{(NL)} := \boldsymbol{\chi}^{(1)}\mathbf{E} + \mathbf{P}^{(NL)}$. Similarly, with $\boldsymbol{\varepsilon} := \mathbf{I} + 4\pi\boldsymbol{\chi}^{(1)}$, the electric displacement field can be decomposed as

$$\mathbf{D} = \boldsymbol{\varepsilon}\mathbf{E} + 4\pi\mathbf{P}^{(NL)}. \tag{1}$$

Furthermore, if the media under consideration are nonmagnetic, isotropic and transversely inhomogeneous w.r.t. z, i.e., $\boldsymbol{\varepsilon} = \varepsilon^{(L)}\mathbf{I}$ with a scalar, possibly complex-valued function $\varepsilon^{(L)} = \varepsilon^{(L)}(z)$, if the wave is linearly E-polarised, i.e.,

$$\mathbf{E} = (E_1, 0, 0)^\top, \quad \mathbf{H} = (0, H_2, H_3)^\top, \tag{2}$$

and if the electric field $\mathbf{E}$ is homogeneous w.r.t. the coordinate x, i.e., $\mathbf{E}(\mathbf{r}, t) = (E_1(t; y, z), 0, 0)^\top$, then the Maxwell's equations together with (1) reduce to

$$\nabla^2\mathbf{E} - \frac{\varepsilon^{(L)}}{c^2}\frac{\partial^2}{\partial t^2}\mathbf{E} - \frac{4\pi}{c^2}\frac{\partial^2}{\partial t^2}\mathbf{P}^{(NL)} = 0, \tag{3}$$

where $\nabla^2 := \partial^2/\partial y^2 + \partial^2/\partial z^2$.

A stationary electromagnetic wave (with oscillation frequency $\omega > 0$) propagating in a weakly nonlinear dielectric structure gives rise to a field containing all frequency harmonics (see [1, 21]). Therefore, representing $\mathbf{E}, \mathbf{P}^{(NL)}$ via Fourier series ($\mathbf{F} \in \{\mathbf{E}, \mathbf{P}^{(NL)}\}$)

$$\mathbf{F}(\mathbf{r}, t) = \frac{1}{2}\sum_{n\in\mathbb{Z}} \mathbf{F}(\mathbf{r}, n\omega)e^{-in\omega t},$$

we obtain from (3) an infinite system of coupled equations w.r.t. the Fourier amplitudes. In the case of a three-component E-polarised electromagnetic field (cf. (2)) this system reduces to a system of scalar equations w.r.t. E_1:

$$\nabla^2 E_1(\mathbf{r}, s\omega) + \frac{\varepsilon^{(L)}(s\omega)^2}{c^2}E_1(\mathbf{r}, s\omega) + \frac{4\pi(s\omega)^2}{c^2}P_1^{(NL)}(\mathbf{r}, s\omega) = 0, \quad s \in \mathbb{N}. \tag{4}$$

We assume that the main contribution to the nonlinearity is introduced by the term $\mathbf{P}^{(NL)}(\mathbf{r}, s\omega)$ (cf. [3–6, 11, 13, 14, 17, 19, 23, 24]), and we take only the lowest-order terms in the Taylor series expansion of the nonlinear part $\mathbf{P}^{(NL)}(\mathbf{r}, s\omega) = (P_1^{(NL)}(\mathbf{r}, s\omega), 0, 0)^\top$ of the polarisation vector in the vicinity of the zero value of the electric field intensity. In this case, the only nontrivial component of the polarisation vector is determined by the susceptibility tensor $\boldsymbol{\chi}^{(3)} = \{\chi^{(3)}_{ijkl}\}^3_{i,j,k,l=1}$, and we have that

$$\begin{aligned} &P_1^{(NL)}(\mathbf{r}, s\omega) \\ &\doteq \frac{1}{4}\sum_{j\in\mathbb{N}} 3\chi^{(3)}_{1111}(s\omega; j\omega, -j\omega, s\omega)|E_1(\mathbf{r}, j\omega)|^2 E_1(\mathbf{r}, s\omega) \end{aligned}$$

$$+\frac{1}{4}\sum_{\substack{n,m,p\in\mathbb{Z}\setminus\{0\}\\ n\neq -m,\ p=s\\ m\neq -p,\ n=s\\ n\neq -p,\ m=s\\ n+m+p=s}}\chi^{(3)}_{1111}(s\omega;n\omega,m\omega,p\omega)E_1(\mathbf{r},n\omega)E_1(\mathbf{r},m\omega)E_1(\mathbf{r},p\omega), \quad (5)$$

where the symbol $\dot{=}$ means that higher-order terms are neglected.

If we study nonlinear effects involving the waves at the first three frequency components of E_1 only, it is possible to restrict the system (4), (5) to three equations. Then the analysis of the scattering problem for the plane wave packet

$$\left\{E_1^{\rm inc}(\mathbf{r},n\kappa):=E_1^{\rm inc}(n\kappa;y,z):=a_{n\kappa}^{\rm inc}\exp\left(i\left(\phi_{n\kappa}y-\Gamma_{n\kappa}(z-2\pi\delta)\right)\right)\right\}_{n=1}^{3}, \quad (6)$$

$z>2\pi\delta$, $\delta>0$, with amplitudes $a_{n\kappa}^{\rm inc}$, angles of incidence $\varphi_{n\kappa}$, $|\varphi|<\pi/2$ (cf. Figure 1) and $\kappa:=\omega/c=2\pi/\lambda$, $\phi_{n\kappa}:=n\kappa\sin\varphi_{n\kappa}$, $\Gamma_{n\kappa}:=\sqrt{(n\kappa)^2-\phi_{n\kappa}^2}$, on the nonlinear structure can be simplified by means of *Kleinman's rule* (i.e., the equality of all the coefficients $\chi^{(3)}_{1111}$ at the multiple frequencies, [10, 12]) and reduces finally to the following system of boundary-value problems ([4–6, 11, 17]):

$$\begin{aligned}
&\left[\nabla^2+\kappa^2\varepsilon_\kappa(z,\alpha(z),E_1(\mathbf{r},\kappa),E_1(\mathbf{r},2\kappa),E_1(\mathbf{r},3\kappa))\right]\times E_1(\mathbf{r},\kappa)\\
&=-\alpha(z)\kappa^2E_1^2(\mathbf{r},2\kappa)\bar{E}_1(\mathbf{r},3\kappa),\\
&\left[\nabla^2+(2\kappa)^2\varepsilon_{2\kappa}(z,\alpha(z),E_1(\mathbf{r},\kappa),E_1(\mathbf{r},2\kappa),E_1(\mathbf{r},3\kappa))\right]\times E_1(\mathbf{r},2\kappa)=0,\\
&\left[\nabla^2+(3\kappa)^2\varepsilon_{3\kappa}(z,\alpha(z),E_1(\mathbf{r},\kappa),E_1(\mathbf{r},2\kappa),E_1(\mathbf{r},3\kappa))\right]\times E_1(\mathbf{r},3\kappa)\\
&=-\alpha(z)(3\kappa)^2\left\{\frac{1}{3}E_1^3(\mathbf{r},\kappa)+E_1^2(\mathbf{r},2\kappa)\bar{E}_1(\mathbf{r},\kappa)\right\},
\end{aligned} \quad (7)$$

where $\kappa:=\omega/c=2\pi/\lambda$,

$$\varepsilon_{n\kappa}:=\begin{cases}\varepsilon^{(L)}+\varepsilon^{(NL)}_{n\kappa}, & |z|\le 2\pi\delta,\\ 1, & |z|>2\pi\delta,\end{cases}\qquad\text{and}\quad \varepsilon^{(L)}:=1+4\pi\chi^{(1)}_{11},$$

$$\begin{aligned}
\varepsilon^{(NL)}_{n\kappa}:=\alpha(z)\Bigg[&|E_1(\mathbf{r},\kappa)|^2+|E_1(\mathbf{r},2\kappa)|^2+|E_1(\mathbf{r},3\kappa)|^2\\
&+\delta_{n1}\frac{\left[\bar{E}_1(\mathbf{r},\kappa)\right]^2}{E_1(\mathbf{r},\kappa)}E_1(\mathbf{r},3\kappa)+\delta_{n2}\frac{\bar{E}_1(\mathbf{r},2\kappa)}{E_1(\mathbf{r},2\kappa)}E_1(\mathbf{r},\kappa)E_1(\mathbf{r},3\kappa)\Bigg]
\end{aligned}$$

with $\alpha(z):=3\pi\chi^{(3)}_{1111}(z)$ and δ_{nm} — Kronecker's symbol. In addition, the following conditions are met ($n=1,\ 2,\ 3$):

(C1) $E_1(n\kappa;y,z)=U(n\kappa;z)\exp(i\phi_{n\kappa}y)$,
(the quasi-homogeneity condition w.r.t. y),

(C2) $\phi_{n\kappa} = n\phi_\kappa$ (or the equivalent condition $\varphi_{n\kappa} = \varphi_\kappa$), (the condition of phase synchronism of waves, see [5]),

(C3) The tangential components $\mathbf{E}_{\mathrm{tg}}(n\kappa; y, z)$ and $\mathbf{H}_{\mathrm{tg}}(n\kappa; y, z)$ of the intensity vectors (i.e., $E_1(n\kappa;\, y,\, z)$ and $H_2(n\kappa;\, y,\, z)$) are continuous at the interfaces $|z| = 2\pi\delta$,

(C4) $E_1^{\mathrm{scat}}(n\kappa; y, z) = \begin{Bmatrix} a_{n\kappa}^{\mathrm{scat}} \\ b_{n\kappa}^{\mathrm{scat}} \end{Bmatrix} \exp(i(\phi_{n\kappa} y \pm \Gamma_{n\kappa}(z \mp 2\pi\delta))),\ z \gtrless \pm 2\pi\delta$ (the radiation condition).

The condition (C4) provides a physically consistent behaviour of the energy characteristics of scattering and guarantees the absence of waves coming from infinity (i.e., $z = \pm\infty$), see [16]. The desired solution is of the form ($n = 1,\, 2,\, 3$):

$$E_1(n\kappa; y, z) = U(n\kappa; z)\exp(i\phi_{n\kappa} y) = \begin{cases} a_{n\kappa}^{\mathrm{inc}} \exp(i(\phi_{n\kappa} y - \Gamma_{n\kappa}(z - 2\pi\delta))) \\ +a_{n\kappa}^{\mathrm{scat}} \exp(i(\phi_{n\kappa} y + \Gamma_{n\kappa}(z - 2\pi\delta))), & z > 2\pi\delta, \\ U(n\kappa; z)\exp(i\phi_{n\kappa} y), & |z| \le 2\pi\delta, \\ b_{n\kappa}^{\mathrm{scat}} \exp(i(\phi_{n\kappa} y - \Gamma_{n\kappa}(z + 2\pi\delta))), & z < -2\pi\delta. \end{cases} \tag{8}$$

Substituting this representation into (7), the following system of nonlinear ordinary differential equations results ($n = 1,\, 2,\, 3$):

$$\begin{aligned} & U''(n\kappa; z) + \big\{\Gamma_{n\kappa}^2 - (n\kappa)^2 \\ & \big[1 - \varepsilon_{n\kappa}(z, \alpha(z), U(\kappa; z), U(2\kappa; z), U(3\kappa; z))\big]\big\} U(n\kappa; z) \\ & = -(n\kappa)^2 \alpha(z)\big(\delta_{n1} U^2(2\kappa; z)\bar{U}(3\kappa; z) \\ & \quad + \delta_{n3}\big\{\frac{1}{3} U^3(\kappa; z) + U^2(2\kappa; z)\bar{U}(\kappa; z)\big\}\big), \quad |z| < 2\pi\delta. \end{aligned} \tag{9}$$

By elementary calculations, from (C3) we obtain the boundary conditions ($n = 1, 2, 3$):

$$\begin{aligned} & i\Gamma_{n\kappa} U(n\kappa; -2\pi\delta) + U'(n\kappa; -2\pi\delta) = 0, \\ & i\Gamma_{n\kappa} U(n\kappa; 2\pi\delta) - U'(n\kappa; 2\pi\delta) = 2i\Gamma_{n\kappa} a_{n\kappa}^{\mathrm{inc}}. \end{aligned} \tag{10}$$

The system of ordinary differential Equation (9) and the boundary conditions (10) form a semi-linear boundary-value problem of Sturm-Liouville type, see also [4–6, 17, 18, 24].

The problem (7), (C1)–(C4) can also be reduced to finding solutions of one-dimensional nonlinear integral equations w.r.t. $U(n\kappa; \cdot) \in L_2(-2\pi\delta, 2\pi\delta)$, $n = 1,\, 2,\, 3$, cf. [4–6, 11, 16–18, 24]:

$$\begin{aligned} & U(n\kappa; z) + \frac{i(n\kappa)^2}{2\Gamma_{n\kappa}} \int_{-2\pi\delta}^{2\pi\delta} \exp(i\Gamma_{n\kappa}|z - \xi|) \\ & \times\big[1 - \varepsilon_{n\kappa}\big(\xi,\ \alpha(\xi), U(\kappa; \xi)\ , U(2\kappa; \xi)\ , U(3\kappa; \xi)\big)\big] U(n\kappa; \xi) d\xi \end{aligned}$$

$$
\begin{aligned}
&= \delta_{n1}\frac{i(n\kappa)^2}{2\Gamma_{n\kappa}}\int_{-2\pi\delta}^{2\pi\delta}\exp(i\Gamma_{n\kappa}|z-\xi|)\alpha(\xi)U^2(2\kappa;\xi)\bar{U}(3\kappa;\xi)d\xi\\
&\quad+\delta_{n3}\frac{i(n\kappa)^2}{2\Gamma_{n\kappa}}\int_{-2\pi\delta}^{2\pi\delta}\exp(i\Gamma_{n\kappa}|z-\xi|)\\
&\quad\times\alpha(\xi)\left\{\frac{1}{3}U^3(\kappa;\xi)+U^2(2\kappa;\xi)\bar{U}(\kappa;\xi)\right\}d\xi\\
&\quad+U^{\mathrm{inc}}(n\kappa;z),\quad |z|\le 2\pi\delta,\quad n=1,2,3. \qquad (11)
\end{aligned}
$$

Here $U^{\mathrm{inc}}(n\kappa;z)=a_{n\kappa}^{\mathrm{inc}}\exp\left[-i\Gamma_{n\kappa}(z-2\pi\delta)\right]$. The following result can be proved.

Theorem 1 *Assume that $\varepsilon^{(L)}$, α are piecewise continuous, bounded and that all the data κ, δ, φ, $\{a_{n\kappa}^{inc}\}_{n=1}^3$, α, and $\varepsilon^{(L)}$ satisfy*

$$
492\gamma\max_{|z|\le 2\pi\delta}|1-\varepsilon^{(L)}(z)|\le 35,\quad \max_{|z|\le 2\pi\delta}|\alpha(z)|\sum_{m=1}^{3}(a_{m\kappa}^{inc})^2\le\frac{1721-2\sqrt{10}}{551368\gamma}
$$

with $\gamma:=\pi\delta\kappa/\cos\varphi$. Then the iteration

$$
\begin{aligned}
&U_{s+1}(n\kappa;z)+\frac{i(n\kappa)^2}{2\Gamma_{n\kappa}}\int_{-2\pi\delta}^{2\pi\delta}\exp(i\Gamma_{n\kappa}|z-\xi|)\\
&\times[1-\varepsilon_{n\kappa}(\xi,\alpha(\xi),U_s(\kappa;\xi),U_s(2\kappa;\xi),U_s(3\kappa;\xi))]U_{s+1}(n\kappa;\xi)d\xi\\
&=\delta_{n1}\frac{i(n\kappa)^2}{2\Gamma_{n\kappa}}\int_{-2\pi\delta}^{2\pi\delta}\exp(i\Gamma_{n\kappa}|z-\xi|)\alpha(\xi)U_s^2(2\kappa;\xi)\bar{U}_s(3\kappa;\xi)d\xi\\
&\quad+\delta_{n3}\frac{i(n\kappa)^2}{2\Gamma_{n\kappa}}\int_{-2\pi\delta}^{2\pi\delta}\exp(i\Gamma_{n\kappa}|z-\xi|)\\
&\quad\times\alpha(\xi)\left\{\frac{1}{3}U_s^3(\kappa;\xi)+U_s^2(2\kappa;\xi)\bar{U}_s(\kappa;\xi)\right\}d\xi\\
&\quad+U^{inc}(n\kappa;z),\quad |z|\le 2\pi\delta,\quad n=1,2,3,\quad s=0,1,2,\ldots,
\end{aligned}
$$

converges for sufficiently small initial values $\{U_0(n\kappa;\cdot)\}_{n=1}^3$ such that $\max_{|z|\le 2\pi\delta}\sum_{m=1}^{3}|U_0(m\kappa;z)|^2\le 1/(82\gamma\max_{|z|\le 2\pi\delta}|\alpha(z)|)$ to the unique solution of the system (11).

3. NUMERICAL INVESTIGATION OF THE NONLINEAR INTEGRAL EQUATIONS AND SPECTRAL PROBLEMS

The application of suitable quadrature rules to the system of nonlinear integral Equation (11) as described in [4–6] leads to a system of

complex-valued nonlinear algebraic equations:

$$\begin{aligned}(\mathbf{I}-\mathbf{B}_{\kappa}(\mathbf{U}_{\kappa},\mathbf{U}_{2\kappa},\mathbf{U}_{3\kappa}))\mathbf{U}_{\kappa}&=\mathbf{C}_{\kappa}(\mathbf{U}_{2\kappa},\mathbf{U}_{3\kappa})+\mathbf{U}_{\kappa}^{\mathrm{inc}},\\ (\mathbf{I}-\mathbf{B}_{2\kappa}(\mathbf{U}_{\kappa},\mathbf{U}_{2\kappa},\mathbf{U}_{3\kappa}))\mathbf{U}_{2\kappa}&=\mathbf{U}_{2\kappa}^{\mathrm{inc}},\\ (\mathbf{I}-\mathbf{B}_{3\kappa}(\mathbf{U}_{\kappa},\mathbf{U}_{2\kappa},\mathbf{U}_{3\kappa}))\mathbf{U}_{3\kappa}&=\mathbf{C}_{3\kappa}(\mathbf{U}_{\kappa},\mathbf{U}_{2\kappa})+\mathbf{U}_{3\kappa}^{\mathrm{inc}},\end{aligned} \tag{12}$$

where we use a discrete set $\{z_l\}_{l=1}^{N}$ of nodes such that $-2\pi\delta =: z_1 < z_2 < \ldots < z_l < \ldots < z_N =: 2\pi\delta$. $\mathbf{U}_{n\kappa} := \{U_l(n\kappa)\}_{l=1}^{N} \approx \{U(n\kappa; z_l)\}_{l=1}^{N}$ and $\mathbf{B}_{n\kappa}(\mathbf{U}_{\kappa},\mathbf{U}_{2\kappa},\mathbf{U}_{3\kappa})$ are the matrices generated by the quadrature method. The right-hand side of (12) is defined by

$$\mathbf{U}_{n\kappa}^{\mathrm{inc}} := \left\{a_{n\kappa}^{\mathrm{inc}}\exp[-i\Gamma_{n\kappa}(z_l-2\pi\delta)]\right\}_{l=1}^{N},$$

$$\mathbf{C}_{\kappa}(\mathbf{U}_{2\kappa},\mathbf{U}_{3\kappa}) := \left\{\frac{i\kappa^2}{2\Gamma_{\kappa}}\sum_{m=1}^{N}A_m\exp(i\Gamma_{\kappa}|z_l-z_m|)\times\alpha(z_m)U_m^2(2\kappa)\bar{U}_m(3\kappa)\right\}_{l=1}^{N},$$

$$\mathbf{C}_{3\kappa}(\mathbf{U}_{\kappa},\mathbf{U}_{2\kappa}) := \left\{\frac{i(3\kappa)^2}{2\Gamma_{3\kappa}}\sum_{m=1}^{N}A_m\exp(i\Gamma_{3\kappa}|z_l-z_m|)\times\alpha(z_m)\Big[\frac{1}{3}U_m^3(\kappa)+U_m^2(2\kappa)\bar{U}_m(\kappa)\Big]\right\}_{l=1}^{N},$$

where the numbers A_m are the coefficients determined by the quadrature rule.

The solution of (12) can be found iteratively, where at each step a system of linearised nonlinear complex-valued algebraic equations is solved.

The system of nonlinear integral Equation (11) can be linearised directly by freezing the permittivities $\varepsilon_{n\kappa}$. The analytic continuation of these linearised nonlinear problems into the region of complex values of the frequency parameter allows us to switch to the analysis of spectral problems. That is, the eigen-frequencies and the eigen-fields of the homogeneous linear problems with an *induced* nonlinear permittivity are to be determined. Analogously as above but at the discrete level we obtain a set of independent systems of linear algebraic equations depending nonlinearly on the spectral parameter:

$$(\mathbf{I}-\mathbf{B}_{n\kappa}(\kappa_n))\mathbf{U}_{\kappa_n}=\mathbf{0}, \tag{13}$$

where $\kappa_n \in \Omega_{n\kappa} \subset \mathsf{H}_{n\kappa}$, at $\kappa=\kappa^{\mathrm{inc}}$, $n=1,2,3$, $\Omega_{n\kappa}$ are the discrete sets of eigen-frequencies and $\mathsf{H}_{n\kappa}$ denote two-sheeted Riemann surfaces

(see [6] and Figure 2). $\mathbf{B}_{n\kappa}(\kappa_n) := \mathbf{B}_{n\kappa}(\kappa_n; \mathbf{U}_\kappa, \mathbf{U}_{2\kappa}, \mathbf{U}_{3\kappa})$ for $\mathbf{U}_{n\kappa}$ given. The spectral problem of finding the eigen-frequencies κ_n and the corresponding eigen-fields $\mathbf{U}_{\kappa_n}$ (i.e., the nontrivial solutions of the linearized homogeneous integral equations) reduces to the following equations:

$$\begin{cases} f_{n\kappa}(\kappa_n) := \det(\mathbf{I} - \mathbf{B}_{n\kappa}(\kappa_n)) = 0, \\ (\mathbf{I} - \mathbf{B}_{n\kappa}(\kappa_n))\mathbf{U}_{\kappa_n} = \mathbf{0}, \\ \kappa := \kappa^{\text{inc}}, \qquad\qquad \kappa_n \in \Omega_{n\kappa} \subset \mathsf{H}_{n\kappa}, \quad n = 1,2,3. \end{cases} \tag{14}$$

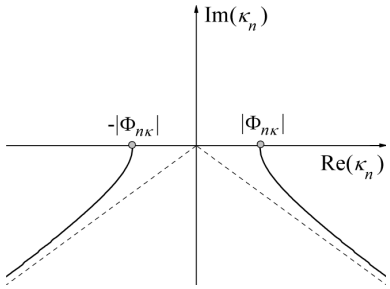

Figure 2. The two-sheeted Riemann surfaces $\mathsf{H}_{n\kappa}$.

4. NUMERICAL RESULTS

Consider the excitation of the nonlinear structure by a strong incident field at the basic frequency κ and, in addition, by weak incident quasi-homogeneous electromagnetic fields at the double and triple frequencies 2κ, 3κ (see (6)), i.e.,

$$0 < \max\left\{\left|a_{2\kappa}^{\text{inc}}\right|, \left|a_{3\kappa}^{\text{inc}}\right|\right\} \ll |a_{1\kappa}^{\text{inc}}|. \tag{15}$$

The desired solution of the scattering and generation problem (7), (C1)–(C4) (or of the equivalent problem (11)) are represented as in (8). The solution of (12) is obtained by means of successive approximations using the self-consistent approach based on an iterative algorithm. In contrast to other techniques such as, e.g., the preset-field method, the self-consistent approach is characterized by the direct application of a numerical solver for nonlinear algebraic equation systems to (12). For a comparison of different possibilities to solve the system (12) the reader is referred to [8].

In order to describe the scattering and generation properties of the nonlinear structure in the zones of reflection $z > 2\pi\delta$ and transmission

$z < -2\pi\delta$, we introduce the following notation:

$$R_{n\kappa} := \left|a_{n\kappa}^{\text{scat}}\right|^2 / \sum_{n=1}^{3} \left|a_{n\kappa}^{\text{inc}}\right|^2 \quad \text{and} \quad T_{n\kappa} := |b_{n\kappa}^{\text{scat}}|^2 / \sum_{n=1}^{3} |a_{n\kappa}^{\text{inc}}|^2,$$

$n = 1, 2, 3$. The quantities $R_{n\kappa}$, $T_{n\kappa}$ are called *reflection, transmission* or *generation coefficients* of the waves w.r.t. the total intensity of the incident packet.

We note that, for nonabsorbing media with $\mathfrak{Im}[\varepsilon^{(L)}(z)] = 0$, the energy balance equation

$$\sum_{n=1}^{3} \left[R_{n\kappa} + T_{n\kappa}\right] = 1 \tag{16}$$

is satisfied. This equation generalises the law of conservation of energy which has been treated in [16, 20] for the case of a single incident field and a single equation. If we define by

$$W_{n\kappa} := \left|a_{n\kappa}^{\text{scat}}\right|^2 + \left|b_{n\kappa}^{\text{scat}}\right|^2$$

the total energy of the scattered and generated fields at the frequencies $n\kappa$, $n = 1, 2, 3$, then the energy balance Equation (16) can be rewritten as

$$\sum_{n=1}^{3} W_{n\kappa} = \sum_{n=1}^{3} \left|a_{n\kappa}^{\text{inc}}\right|^2 .$$

In the numerical experiments, the quantities $W_{3\kappa}/W_{\kappa}$ (which characterises the portion of energy generated in the third harmonic in comparison to the energy scattered in the nonlinear layer) and

$$W^{(\text{Error})} := 1 - \sum_{n=1}^{3} \left[R_{n\kappa} + T_{n\kappa}\right] \tag{17}$$

(which characterises the numerical violation of the energy balance) are of particular interest. We emphasize that in the numerical simulation of scattering and generation processes without any weak fields, i.e., $a_{2\kappa}^{\text{inc}} = a_{3\kappa}^{\text{inc}} = 0$, the residual of the energy balance Equation (16) does not exceed the value $|W^{(\text{Error})}| < 10^{-8}$. However, taking into consideration the impact of weak fields in the numerical simulation of the same scattering and generation processes, i.e., $a_{n\kappa}^{\text{inc}} \neq 0$, $n = 2, 3$, the error in the balance Equation (16) can reach up to several percent. This indicates that the intensities of the exciting weak fields are sufficiently large such that these fields become also sources for the generation of oscillations. For such situations, the presented mathematical model (7), (C1)–(C4) and the linearised

nonlinear spectral problems should take into account the complex Fourier amplitudes of the oscillations at the frequencies $n\kappa$ for numbers $n > 3$. Furthermore we observe, on the one hand, situations in which the influence of a weak field $a_{2\kappa}^{\text{inc}} \neq 0$ on the scattering and generation process of oscillations leads to small errors in the energy balance Equation (16) not exceeding 2% (that is $|W^{(\text{Error})}| < 0.02$), and, on the other hand, situations in which the error can reach 6% (that is $|W^{(\text{Error})}| < 0.06$ there, where in the region of generation of oscillations the condition (15) is violated). The scattering, generating, energetic, and dielectric properties of the nonlinear layer are illustrated by surfaces in dependence on the parameters of the particular problem. The bottom chart depicts the surface of the value of the residual $W^{(\text{Error})}$ of the energy balance Equation (see (17)) and its projection onto the top horizontal plane of the figure. In particular, by the help of these graphs it is easy to localise that region of parameters of the problem, where the error of the energy balance does not exceed a given value, that is $|W^{(\text{Error})}| < \text{const}$.

The spectral characteristics of the linearised nonlinear problems with the induced dielectric permittivity at the frequencies $n\kappa$, $n = 1, 2, 3$, of excitation and generation were calculated by means of the algorithm (14). In the graphical illustration of the eigen-fields $\mathbf{U}_{\kappa_n}$ we have set $a_{\kappa_n} := 1$ for $\kappa_n \in \Omega_{n\kappa} \subset \mathsf{H}_{n\kappa}$, $n = 1, 2, 3$. Finally we mention that the later-used classification of scattered, generated or eigen-fields of the dielectric layer by the $H_{m,l,p}$-type is identical to that given in [15, 16, 22]. In the case of E-polarisation, $H_{m,l,p}$ (or $TE_{m,l,p}$) denotes the type of polarisation of the wave field under investigation. The subscripts indicate the number of local maxima of $|E_1|$ (or $|U|$, as $|E_1| = |U|$) along the coordinate axes x, y and z (see Figure 1). Since the considered waves are homogeneous along the x-axis and quasi-homogeneous along the y-axis, we study actually fields of the type $H_{0,0,p}$ (or $TE_{0,0,p}$), where the subscript p is equal to the number of local maxima of the function $|U|$ of the argument $z \in [-2\pi\delta, 2\pi\delta]$.

In what follows we will consider a single-layered structure with a dielectric permittivity $\varepsilon_{n\kappa}(z, \alpha(z), U(\kappa; z), U(2\kappa; z), U(3\kappa; z)) = \varepsilon^{(L)}(z) + \varepsilon_{n\kappa}^{(NL)}$, $n = 1, 2, 3$, where $\varepsilon^{(L)}(z) := 16$ and $\alpha(z) := \mp 0.01$ for $z \in [-2\pi\delta, 2\pi\delta]$, $\delta := 0.5$, $\kappa^{\text{inc}} := \kappa := 0.375$, and $\varphi_\kappa \in [0°, 90°)$. In the subsequent figures we will use the following conventions to illustrate the different cases of incident fields:

$a_{2\kappa}^{\text{inc}} = \frac{1}{3} a_{\kappa}^{\text{inc}}, a_{3\kappa}^{\text{inc}} = 0$ ... graphs labeled by "1/3",
$a_{2\kappa}^{\text{inc}} = \frac{2}{3} a_{\kappa}^{\text{inc}}, a_{3\kappa}^{\text{inc}} = 0$ ... graphs labeled by "2/3",
$a_{2\kappa}^{\text{inc}} = a_{3\kappa}^{\text{inc}} = 0$ ... graphs labeled by "0".

4.1. A Single-layered Structure with a Negative Value of the Cubic Susceptibility

The Figure 3–Figure 6 demonstrate the electrodynamical properties of a nonlinear decanalising layer with a constant cubic susceptibility $\alpha(z) := -0.01$.

The results shown in Figure 3 allow us to understand the dynamical behaviour of the quantity $W_{3\kappa}/W_\kappa$ characterising the ratio of the generated and scattered energies. Figure 3 shows the dependence of $W_{3\kappa}/W_\kappa$ on the angle of incidence φ_κ and on the amplitude a_κ^{inc} of the incident field for the case $a_{2\kappa}^{\mathrm{inc}} = \frac{2}{3}a_\kappa^{\mathrm{inc}}$. It describes the portion of energy generated in the third harmonic by the nonlinear layer when a plane wave at the excitation frequency κ and with the amplitude a_κ^{inc} is passing the layer under the angle of incidence φ_κ. For example, in Figure 3(a) the maximum value of $W_{3\kappa}/W_\kappa$ and the value $W^{(\mathrm{Error})}$ are reached at the following parameters $[a_\kappa^{\mathrm{inc}}, a_{2\kappa}^{\mathrm{inc}}, \varphi_\kappa]$: $W_{3\kappa}/W_\kappa = 0.08075$, $W^{(\mathrm{Error})} = -0.03207$, $[a_\kappa^{\mathrm{inc}} = 24, a_{2\kappa}^{\mathrm{inc}} = \frac{2}{3}a_\kappa^{\mathrm{inc}}, \varphi_\kappa = 0°]$ . . . graph #2/3. The results depicted in Figure 3(a) show that the maximal portion of the total energy generated in the third harmonic is observed in the direction normal to the structure, cf. the behaviour of the surfaces $W_{3\kappa}/W_\kappa$ at $\varphi_\kappa = 0°$.

The right diagram in Figure 3 displays some graphs characterising the scattering and generation properties of the nonlinear structure. Graph #0.0 illustrates the value of the linear part $\varepsilon^{(L)} = 16$ of the permittivity of the nonlinear layered structure. Graphs $\#\,n.1$ and $\#\,n.2$ show the real and imaginary parts of the permittivities at the frequencies $n\kappa$, $n = 1, 2, 3$. The figure also shows the absolute values

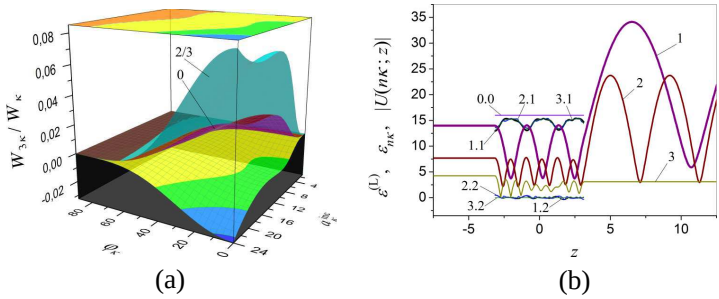

(a) (b)

Figure 3. The portion of energy generated in the third harmonic for (a) $a_{2\kappa}^{\mathrm{inc}} = \frac{2}{3}a_\kappa^{\mathrm{inc}}$ and (b) some graphs describing the properties of the nonlinear layer for $\varphi_\kappa = 0°$, $a_\kappa^{\mathrm{inc}} = 20$ and $a_{2\kappa}^{\mathrm{inc}} = \frac{2}{3}a_\kappa^{\mathrm{inc}}$: $\#0.0, \ldots, \varepsilon^{(L)}$, $\#1, \ldots, |U(\kappa; z)|$, $\#2, \ldots, |U(2\kappa; z)|$, $\#3, \ldots, |U(3\kappa; z)|$, $\#\,n.1, \ldots, \mathfrak{Re}(\varepsilon_{n\kappa})$, $\#\,n.2, \ldots, \mathfrak{Im}(\varepsilon_{n\kappa})$.

$|U(\kappa;z)|$, $|U(2\kappa;z)|$ of the amplitudes of the full scattered fields at the frequencies of excitation κ, 2κ (graphs #1, #2) and $|U(3\kappa;z)|$ of the generated field at the frequency 3κ (graph #3). The values $|U(n\kappa;z)|$ are given in the nonlinear layered structure ($|z| \le 2\pi\delta$) and outside it (i.e., in the zones of reflection $z > 2\pi\delta$ and transmission $z < -2\pi\delta$). Here $W^{(\mathrm{Error})} = -1.902471 \cdot 10^{-2}$, i.e., the error in the energy balance is less than 1.9% (b).

The nonlinear parts $\varepsilon_{n\kappa}^{(NL)}$ of the dielectric permittivity at each frequency $n\kappa$ depend on the values $U_{n\kappa} := U(n\kappa;z)$, $n = 1,2,3$,

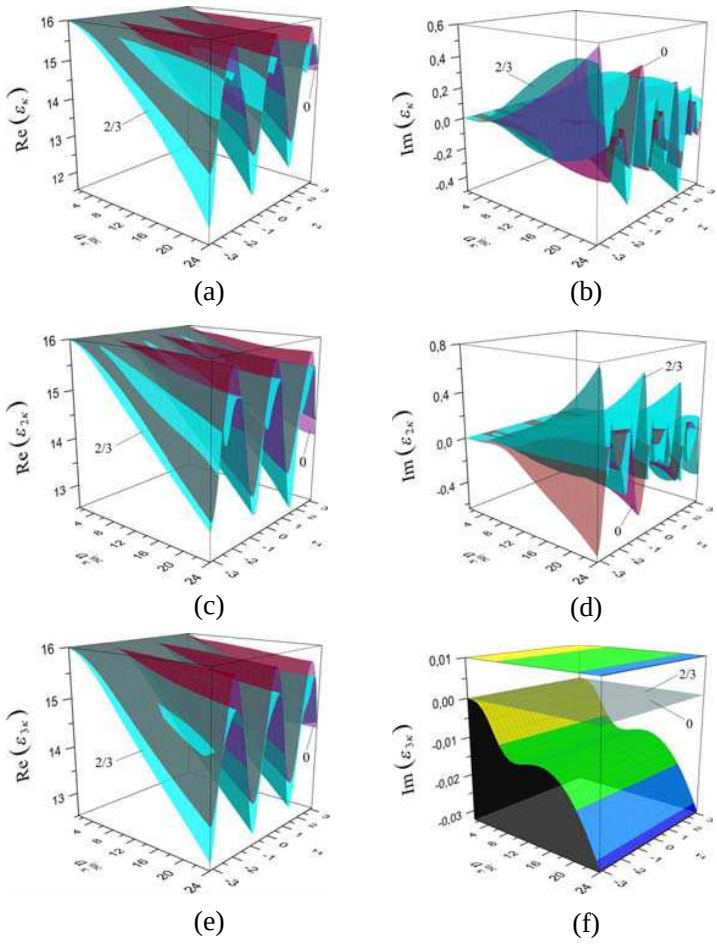

Figure 4. Graphs characterising the nonlinear dielectric permittivity in dependence on $[a_\kappa^{\mathrm{inc}}, a_{2\kappa}^{\mathrm{inc}}, z]$ for $\varphi_\kappa = 0^\circ$ and $a_{2\kappa}^{\mathrm{inc}} = \frac{2}{3} a_\kappa^{\mathrm{inc}}$: (a) $\mathfrak{Re}(\varepsilon_\kappa)$, (b) $\mathfrak{Im}(\varepsilon_\kappa)$, (c) $\mathfrak{Re}(\varepsilon_{2\kappa})$, (d) $\mathfrak{Im}(\varepsilon_{2\kappa})$, (e) $\mathfrak{Re}(\varepsilon_{3\kappa})$, (f) $\mathfrak{Im}(\varepsilon_{3\kappa})$.

of the fields. The variation of the nonlinear parts $\varepsilon_{n\kappa}^{(NL)}$ of the dielectric permittivity for increasing amplitudes $a_{\kappa}^{\mathrm{inc}}$ and $a_{2\kappa}^{\mathrm{inc}}$ of the incident fields are illustrated by the behaviour of $\mathfrak{Re}(\varepsilon_{n\kappa}[a_{\kappa}^{\mathrm{inc}}, a_{2\kappa}^{\mathrm{inc}}, z])$ and $\mathfrak{Im}(\varepsilon_{n\kappa}[a_{\kappa}^{\mathrm{inc}}, a_{2\kappa}^{\mathrm{inc}}, z])$ at the frequencies $n\kappa$ in Figure 4 (case $a_{2\kappa}^{\mathrm{inc}} = \frac{2}{3}a_{\kappa}^{\mathrm{inc}}$). The quantities $\mathfrak{Im}(\varepsilon_{n\kappa})$ take both positive and negative values along the height of the nonlinear layer (i.e., in the interval $z \in [-2\pi\delta, 2\pi\delta]$), see Figures 4(b), (d), (f). For given amplitudes $a_{\kappa}^{\mathrm{inc}}$ and $a_{2\kappa}^{\mathrm{inc}}$, the graph of $\mathfrak{Im}\left(\varepsilon_{n\kappa}\left[a_{\kappa}^{\mathrm{inc}}, a_{2\kappa}^{\mathrm{inc}}, z\right]\right)$ characterises the *loss of energy* in the nonlinear layer at the excitation frequencies $n\kappa$, $n = 1, 2$, caused by the *generation* of the electromagnetic field of the third harmonic. Such a situation arises because of the right-hand side of (7) at the triple frequency and the generation which is evoked by the right-hand side of (7) at the basic frequency. In our case $\mathfrak{Im}[\varepsilon^{(L)}(z)] = 0$ and $\mathfrak{Im}[\alpha(z)] = 0$, therefore,

$$\begin{aligned}
&\mathfrak{Im}(\varepsilon_{n\kappa}(z, \alpha(z), U(\kappa; z), U(2\kappa; z), U(3\kappa; z))) \\
&= \alpha(z)\big[\delta_{n1}|U(\kappa; z)||U(3\kappa; z)| \\
&\quad \times \mathfrak{Im}\left(\exp\left\{i\left[-3\mathrm{arg}(U(\kappa; z)) + \mathrm{arg}(U(3\kappa; z))\right]\right\}\right) \\
&\quad + \delta_{n2}|U(\kappa; z)||U(3\kappa; z)| \\
&\quad \times \mathfrak{Im}\left(\exp\left\{i\left[-2\mathrm{arg}(U(2\kappa; z)) + \mathrm{arg}(U(\kappa; z)) + \mathrm{arg}(U(3\kappa; z))\right]\right\}\right)\big], \\
&\quad n = 1, 2, 3. \qquad (18)
\end{aligned}$$

From Figures 4(b), (d), (f) we see that small values of $a_{\kappa}^{\mathrm{inc}}$ and $a_{2\kappa}^{\mathrm{inc}}$ induce a small amplitude of the function $\mathfrak{Im}(\varepsilon_{n\kappa})$, i.e., $|\mathfrak{Im}(\varepsilon_{n\kappa})| \approx 0$. The increase of $a_{\kappa}^{\mathrm{inc}}$ corresponds to a strong incident field and leads to the generation of a third harmonic field $U(3\kappa; z)$, and the increase of $a_{2\kappa}^{\mathrm{inc}}$ changes the behaviour of $\varepsilon_{n\kappa}$ (compare the surface #0 with the surface #2/3 in Figure 4). Figures 4(b), (d), (f) shows the dynamical behaviour of $\mathfrak{Im}(\varepsilon_{n\kappa})$. It can be seen that $\mathfrak{Im}(\varepsilon_{3\kappa}) = 0$, whereas at the same time the values of $\mathfrak{Im}(\varepsilon_{n\kappa})$, $n = 1, 2$, may be *positive or negative* along the height of the nonlinear layer, i.e., in the interval $z \in [-2\pi\delta, 2\pi\delta]$, see (18). The zero values of $\mathfrak{Im}(\varepsilon_{n\kappa})$, $n = 1, 2$, are determined by the phase relations between the scattered and the generated fields in the nonlinear layer, namely at the basic frequency κ by the phase relation between $U(\kappa; z)$, $U(3\kappa; z)$, and at the double frequency 2κ by the phases of $\{U(n\kappa; z)\}_{n=1,2,3}$, see (18):

$$\begin{aligned}
&\delta_{n1}\left[-3\mathrm{arg}(U(\kappa; z)) + \mathrm{arg}(U(3\kappa; z))\right] \\
&+\delta_{n2}\left[-2\mathrm{arg}(U(2\kappa; z)) + \mathrm{arg}(U(\kappa; z)) + \mathrm{arg}(U(3\kappa; z))\right] = p\pi, \\
&p = 0, \pm 1, \ldots, \quad n = 1, 2.
\end{aligned}$$

We mention that the behaviour of both the quantities $\mathfrak{Im}(\varepsilon_{n\kappa})$ and

$$\begin{aligned}
&\mathfrak{Re}(\varepsilon_{n\kappa}(z,\alpha(z),U(\kappa;z),U(2\kappa;z),U(3\kappa;z))\\
&-\varepsilon_{3\kappa}(z,\alpha(z),U(\kappa;z),U(2\kappa;z),U(3\kappa;z)))\\
&=\alpha(z)\big[\delta_{n1}|U(\kappa;z)||U(3\kappa;z)|\\
&\times\mathfrak{Re}\left(\exp\left\{i\left[-3\arg(U(\kappa;z))+\arg(U(3\kappa;z))\right]\right\}\right)\\
&+\ \delta_{n2}|U(\kappa;z)||U(3\kappa;z)|\times\\
&\times\mathfrak{Re}\left(\exp\left\{i\left[-2\arg(U(2\kappa;z))+\arg(U(\kappa;z))+\arg(U(3\kappa;z))\right]\right\}\right)\big],\\
&n=1,2,
\end{aligned}\tag{19}$$

plays an essential role in the process of third harmonic generation.

We mention that the impact of a strong electromagnetic field with an amplitude $a_\kappa^{\rm inc}$ even in the absence of a weak field $a_{2\kappa}^{\rm inc}=0$ (where $U(2\kappa;z)=0$) induces a nontrivial component of the nonlinear dielectric permittivity at the frequency 2κ. Figures 4(c), (d) show that the existence of nontrivial values $\mathfrak{Re}(\varepsilon_{2\kappa})\neq\mathfrak{Re}(\varepsilon^{(L)})$ and $\mathfrak{Im}(\varepsilon_{2\kappa})\neq 0$ is caused by the amplitude and phase characteristics of the fields $U(\kappa;z)$ and $U(3\kappa;z)$. Moreover, the nonlinear component of the dielectric permittivity, which is responsible for the variation of $\mathfrak{Im}(\varepsilon_{n\kappa})$ (and $\mathfrak{Re}(\varepsilon_{n\kappa}-\varepsilon_{3\kappa})$), does not depend on the absolute value of the amplitude of the field at the double frequency $|U(2\kappa;z)|$, see (19) and (18). Thus, even a weak field includes a mechanism for the redistribution of the energy of the incident wave packet which is consumed for the scattering process and the generation of waves, cf. the dynamics of the surfaces #0 with #2/3 in Figure 4.

The scattering and generation properties of the nonlinear structure in the ranges $a_\kappa^{\rm inc}\in[1,24]$, $a_{2\kappa}^{\rm inc}=\frac{2}{3}a_\kappa^{\rm inc}$ and $\varphi_\kappa=0^\circ$ of the parameters of the incident field are presented in Figures 5&6(a). Figure 5 shows the same dependencies as Figure 6(a) but with the additional parameter $a_{2\kappa}^{\rm inc}$. So it is possible to track the dynamics of the scattering, generation and energy characteristics of the nonlinear layer under the influence of an incident wave package consisting of a strong and a weak magnetic field with amplitudes $a_\kappa^{\rm inc}$ and $a_{2\kappa}^{\rm inc}$, resp.

The graphs in Figure 6 show the dynamics of the scattering ($R_\kappa[\varphi_\kappa,a_\kappa^{\rm inc},a_{2\kappa}^{\rm inc}]$, $T_\kappa[\varphi_\kappa,a_\kappa^{\rm inc},a_{2\kappa}^{\rm inc}]$, $R_{2\kappa}[\varphi_\kappa,a_\kappa^{\rm inc},a_{2\kappa}^{\rm inc}]$, $T_{2\kappa}[\varphi_\kappa,a_\kappa^{\rm inc},a_{2\kappa}^{\rm inc}]$) and generation ($R_{3\kappa}\big[\varphi_\kappa,a_\kappa^{\rm inc},a_{2\kappa}^{\rm inc}\big]$, $T_{3\kappa}\big[\varphi_\kappa,a_\kappa^{\rm inc},a_{2\kappa}^{\rm inc}\big]$) properties of the structure.

In the resonant range of wave scattering and generation frequencies, i.e., $\kappa^{\rm scat}:=\kappa^{\rm inc}=\kappa$ and $\kappa^{\rm gen}=3\kappa$, resp., the dynamical behaviour of the characteristic quantities depicted in Figure 6 has the following causes. The scattering and generation frequencies are close to the corresponding eigen-frequencies of the linear ($\alpha=0$) and linearised nonlinear ($\alpha\neq 0$) spectral problems. Furthermore, the distance

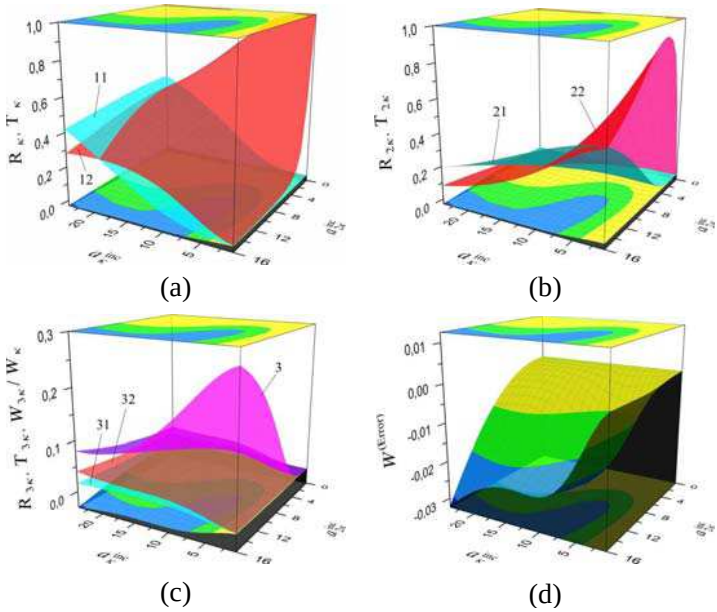

Figure 5. The scattering and generation properties of the nonlinear structure in dependence on $\left[\varphi_\kappa, a_\kappa^{\mathrm{inc}}, a_{2\kappa}^{\mathrm{inc}}\right]$ for $\varphi_\kappa = 0°$: (a) R_κ, T_κ (#11, #12), (b) $R_{2\kappa}$, $T_{2\kappa}$ (#21, #22), (c) $W_{3\kappa}/W_\kappa$, $R_{3\kappa}$, $T_{3\kappa}$ (#3, #31, #32), (d) $W^{(\mathrm{Error})}$.

between the corresponding eigen-frequencies of the spectral problems with $\alpha = 0$ and $\alpha \neq 0$ is small. Thus, the graphs in Figure 6(a) can be compared with the dynamical behaviour of the branches of the eigen-frequencies of the spectral problems presented in Figure 6(b). The graphs of the eigen-fields corresponding to the branches of the considered eigen-frequencies are shown in Figures 6(e), (f).

Let us denote by

$$Q_{\kappa_n} := -\frac{\mathfrak{Re}(\kappa_n)}{2\mathfrak{Im}(\kappa_n)} \tag{20}$$

the Q-factors of the eigenoscillations of the spectral problem (14) at the frequencies $\kappa_n \in \Omega_{n\kappa} \subset H_{n\kappa}$, see [7, 16] and Figure 6(c). In the numerical experiments, the function $Q_{13}(a_{n\kappa}^{\mathrm{inc}}) := Q_{\kappa_1}(a_{n\kappa}^{\mathrm{inc}})/Q_{\kappa_3}(a_{n\kappa}^{\mathrm{inc}})$ of the relative Q-factor of the eigenoscillations is of particular interest, see Figure 6(d). For an increasing amplitude of the exciting field, an increase of the generated energy in the higher harmonics is accompanied by a monotonic decrease of the relative Q-factor of the eigenoscillations, see Figures 6(a) and 6(d).

Figure 6(b) illustrates the dispersion characteristics of the linear

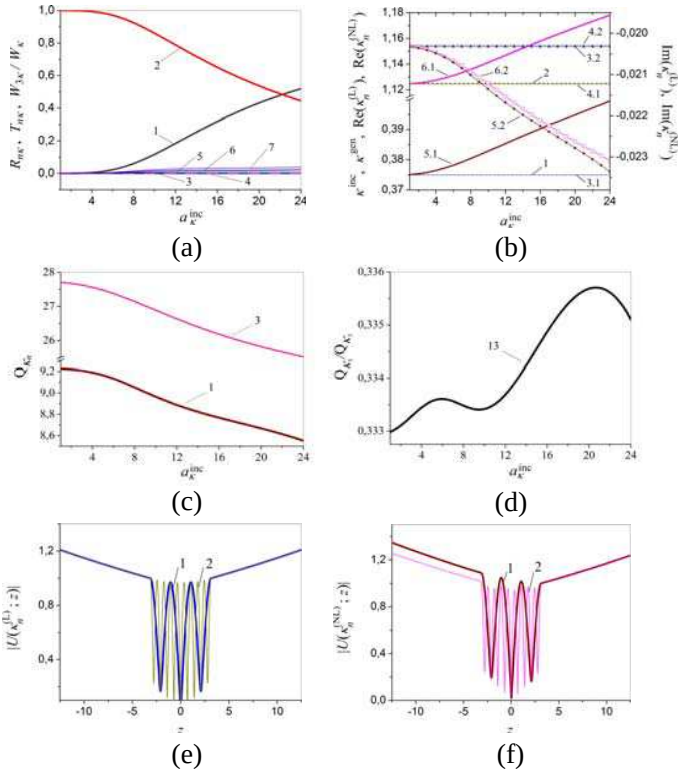

Figure 6. (a) The curves R_κ (#1), T_κ (#2), $R_{2\kappa}$ (#3), $T_{2\kappa}$ (#4), $R_{3\kappa}$ (#5), $T_{3\kappa}$ (#6), $W_{3\kappa}/W_\kappa$ (#7) for $\varphi_\kappa = 0°$; (b) the curves $\kappa := \kappa^{\rm inc} := 0.375$ (#1), $3\kappa = \kappa^{\rm gen} = 3\kappa^{\rm inc} = 1.125$ (#2), the complex eigen-frequencies $\mathfrak{Re}(\kappa_1^{(L)})$ (#3.1), $\mathfrak{Im}(\kappa_1^{(L)})$ (#3.2), $\mathfrak{Re}(\kappa_3^{(L)})$ (#4.1), $\mathfrak{Im}(\kappa_3^{(L)})$ (#4.2) of the linear problem ($\alpha = 0$) and $\mathfrak{Re}(\kappa_1^{(NL)})$ (#5.1), $\mathfrak{Im}(\kappa_1^{(NL)})$ (#5.2), $\mathfrak{Re}(\kappa_3^{(NL)})$ (#6.1), $\mathfrak{Im}(\kappa_3^{(NL)})$ (#6.2) of the linearised nonlinear problem ($\alpha = -0.01$) for $\varphi_\kappa = 0°$; the Q-factors of eigenoscillations of the spectral problem at $\alpha = -0.01$, $\kappa^{\rm inc} = 0.375$, $\varphi_\kappa = 0°$, $\kappa_n = \kappa_n^{(NL)}$: (c) Q_{κ_1} (#1) and (d) Q_{κ_3} (#3), $Q_{\kappa_1}/Q_{\kappa_3}$ (#13); the graphs of the eigen-fields of the layer for $\varphi_\kappa = 0°$, $a_\kappa^{\rm inc} = 20$: (e) the linear problem ($\alpha = 0$,): $|U(\kappa_1^{(L)}; z)|$ with $\kappa_1^{(L)} = 0.3749822 - i\,0.02032115$ (#1), $|U(\kappa_3^{(L)}; z)|$ with $\kappa_3^{(L)} = 1.124512 - i\,0.02028934$ (#2), (f) the linearised nonlinear problem ($\alpha = -0.01$): $|U(\kappa_1^{(NL)}; z)|$ with $\kappa_1^{(NL)} = 0.3949147 - i\,0.02278218$ (#1), $|U(\kappa_3^{(NL)}; z)|$ with $\kappa_3^{(NL)} = 1.168264 - i\,0.02262382$ (#2).

($\alpha = 0$) and the linearised nonlinear ($\alpha = -0.01$) layer $\varepsilon_{n\kappa} = \varepsilon^{(L)} + \varepsilon^{(NL)}_{n\kappa}$, $n = 1, 2, 3$. The nonlinear components of the permittivity at the scattering (excitation) frequencies $\kappa^{\text{scat}} := \kappa^{\text{inc}} = \kappa$ and the generation frequencies $\kappa^{\text{gen}} := 3\kappa$ depend on the amplitude a^{inc}_{κ} and the angle of incidence φ_{κ} of the incident field. This is reflected in the dynamics of the behaviour of the complex-valued eigen-frequencies of the linear and the linearised nonlinear layer.

We start the discussion of the results of our calculations with the comparison of the dispersion relations given by the branches of the eigen-frequencies (curves #3.1, #3.2 and #5.1, #5.2) near the scattering frequency (curve #1, corresponding to the excitation frequency) and (curves #4.1, #4.2, #6.1, #6.2) near the oscillation frequency (line #2) in the situations presented in Figure 6(b). The graph #5.1 lies above the graph #3.1 and the graph #6.1 above the graph #4.1. That is, decanalising properties (properties of transparency) of the nonlinear layer occur if $\alpha < 0$.

Comparing the results shown in Figure 6(a) and Figure 6(b) we note the following. The dynamics of the change of the scattering properties R_{κ}, T_{κ} of the nonlinear layer (compare the behaviour of curves #1 and #2 in Figure 6(a)) depends on the magnitude of the distance between the curves #3.1 and #5.1 in Figure 6(b). Decanelising properties of the layer occur when $\alpha < 0$. A previously transparent (Figure 6(a)) or reflective (Figure 6(b)) structure loses its properties. It becomes transparent and the reflection and transmission coefficients become comparable. The greater the distance between the curves #4.1 and #6.1 (see Figure 6(b)), the greater the values of $R_{3\kappa}$, $T_{3\kappa}$, $W_{3\kappa}/W_{\kappa}$, characterising the generating properties of the nonlinear layer, see Figure 6(a).

The magnitudes of the absolute values of the eigen-fields shown in Figures 6(e), 6(f) correspond to the branches of the eigen-frequencies of the linear and the linearised nonlinear spectral problems, see Figure 6(b). The curves in Figures 6(e), 6(f) are labeled by #1 for an eigen-field of type $H_{0,0,4}$ and by #2 for an eigen-field of type $H_{0,0,10}$. The loss of symmetry in the eigen-fields with respect to the z-axis in Figure 6(f) is due to the violation of the symmetry (w.r.t. the axis $z = 0$) in the induced dielectric permittivity at both the scattering (excitation) and the oscillation frequencies, see Figure 4.

4.2. A Single-layered Structure with a Positive Value of the Cubic Susceptibility

In this subsection we present and discuss results of the numerical analysis of scattering and generation properties as well as the eigen-

modes of the dielectric layer with a positive value of the cubic susceptibility of the medium. The electrodynamical properties of a nonlinear canalising layer are depicted in the Figure 7– Figure 11 for the case of a constant cubic susceptibility $\alpha(z) := +0.01$.

The results shown in Figure 7 allow us to track the dynamical behaviour of the quantity $W_{3\kappa}/W_\kappa$ characterising the ratio of the generated and scattered energies. Figure 7 shows the dependence of $W_{3\kappa}/W_\kappa$ on the angle of incidence φ_κ and on the amplitude a_κ^{inc} of the incident field for different relations between $a_{2\kappa}^{\text{inc}}$ and a_κ^{inc}. It describes the portion of energy generated in the third harmonic by the nonlinear layer when a plane wave at the excitation frequency κ and with the amplitude a_κ^{inc} is passing the layer under the angle of incidence φ_κ. It can be seen that the weaker incident field at the frequency 2κ leads to an increase of $W_{3\kappa}/W_\kappa$ in comparison with the situation where the structure is excited only by a single field at the basic frequency κ. For example, in Figure 7 the maximum value of $W_{3\kappa}/W_\kappa$ and the value $W^{(\text{Error})}$ are reached at the following parameters $[a_\kappa^{\text{inc}}, a_{2\kappa}^{\text{inc}}, \varphi_\kappa]$: $W_{3\kappa}/W_\kappa = 0.08753$, $W^{(\text{Error})} = -1.98292 \cdot 10^{-9}$, $[a_\kappa^{\text{inc}} = 9.93, a_{2\kappa}^{\text{inc}} = 0, \varphi_\kappa = 53°]$ ... graph #0 and, taking into consideration the weak field at the double frequency, $W_{3\kappa}/W_\kappa = 0.13903$, $W^{(\text{Error})} = -0.01692$, $[a_\kappa^{\text{inc}} = 9.93, a_{2\kappa}^{\text{inc}} = \frac{1}{3}a_\kappa^{\text{inc}}, \varphi_\kappa = 53°]$ ... graph #1/3 (a); $W_{3\kappa}/W_\kappa = 0.03265$, $W^{(\text{Error})} = -8.53239 \cdot 10^{-9}$, $[a_\kappa^{\text{inc}} = 8, a_{2\kappa}^{\text{inc}} = 0, \varphi_\kappa = 42°]$ ... graph #0 and, taking into consideration the weak field at the double frequency, $W_{3\kappa}/W_\kappa = 0.1864$, $W^{(\text{Error})} = -0.04625$, $[a_\kappa^{\text{inc}} = 8, a_{2\kappa}^{\text{inc}} = \frac{2}{3}a_\kappa^{\text{inc}}, \varphi_\kappa = 50°]$ ... graph #2/3 (b).

The numerical analysis of the processes displayed in Figure 8(a) by the curves #3 in the range of angles $\varphi_\kappa \in (66°, 79°)$ and #4 in the range of angles $\varphi_\kappa \in (62°, 82°)$ did not lead to the convergence of the computational algorithm. The value $W_{3\kappa}/W_\kappa = 0.3558$ for $a_\kappa^{\text{inc}} = 14$,

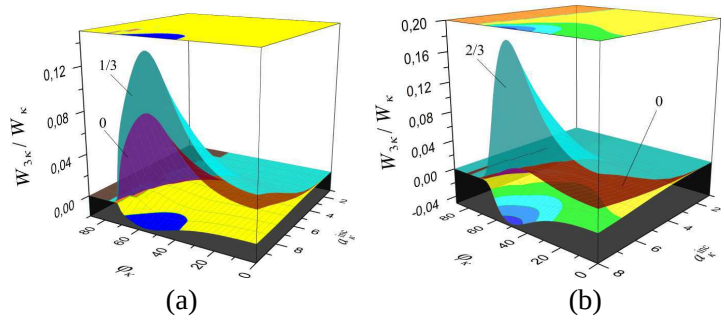

Figure 7. The portion of energy generated in the third harmonic: (a) $a_{2\kappa}^{\text{inc}} = \frac{1}{3}a_\kappa^{\text{inc}}$, (b) $a_{2\kappa}^{\text{inc}} = \frac{2}{3}a_\kappa^{\text{inc}}$.

$a_{2\kappa}^{\text{inc}} = 0$ and $\varphi_\kappa = 66°$ (see the graph #3 in Figure 8(a)) indicates that $W_{3\kappa}$ is 35.58% of W_κ. This is the maximum value of $W_{3\kappa}/W_\kappa$ that has been achieved in the case of a single incident field at the basic frequency κ.

The right diagram in Figure 8 displays some graphs characterising the scattering and generation properties of the nonlinear structure. Graph #0.0 illustrates the value of the linear part $\varepsilon^{(L)} = 16$ of the permittivity of the nonlinear layered structure. Graphs $\#\, n.1$ and $\#\, n.2$ show the real and imaginary parts of the permittivities at the frequencies $n\kappa$, $n = 1, 2, 3$. The figure also shows the absolute values $|U(\kappa; z)|$, $|U(2\kappa; z)|$ of the amplitudes of the full scattered fields at the frequencies of excitation κ, 2κ (graphs #1, #2) and $|U(3\kappa; z)|$ of the generated field at the frequency 3κ (graph #3). The values $|U(n\kappa; z)|$ are given in the nonlinear layered structure ($|z| \le 2\pi\delta$) and outside it (i.e., in the zones of reflection $z > 2\pi\delta$ and transmission $z < -2\pi\delta$). Here $W^{(\text{Error})} = -5.782328 \cdot 10^{-3}$, i.e., the error in the energy balance is less than 0.58% (b).

The nonlinear parts $\varepsilon_{n\kappa}^{(NL)}$ of the dielectric permittivity at each frequency $n\kappa$ depend on the values $U_{n\kappa} := U(n\kappa; z)$, $n = 1, 2, 3$, of the fields. The variation of the nonlinear parts $\varepsilon_{n\kappa}^{(NL)}$ of the dielectric permittivity for increasing amplitudes a_κ^{inc} and $a_{2\kappa}^{\text{inc}}$ of the incident fields are illustrated by the behaviour of $\mathfrak{Re}(\varepsilon_{n\kappa}[a_\kappa^{\text{inc}}, a_{2\kappa}^{\text{inc}}, z])$ and $\mathfrak{Im}(\varepsilon_{n\kappa}[a_\kappa^{\text{inc}}, a_{2\kappa}^{\text{inc}}, z])$ at the frequencies $n\kappa$ in Figure 9 for the case $a_{2\kappa}^{\text{inc}} = \frac{1}{3} a_\kappa^{\text{inc}}$. The quantities $\mathfrak{Im}(\varepsilon_{n\kappa})$ take both positive and negative values along the height of the nonlinear layer (i.e., in the interval

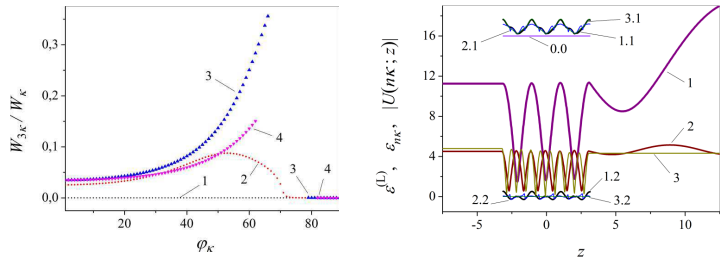

Figure 8. The portion of energy generated in the third harmonic: (a) #1 ,..., $a_\kappa^{\text{inc}} = 1$, #2, ..., $a_\kappa^{\text{inc}} = 9.93$, #3, ..., $a_\kappa^{\text{inc}} = 14$, #4, ..., $a_\kappa^{\text{inc}} = 19$ for $a_{2\kappa}^{\text{inc}} = 0$, some graphs describing the properties of the nonlinear layer for $\varphi_\kappa = 60°$, $a_\kappa^{\text{inc}} = 14$ and (b) $a_{2\kappa}^{\text{inc}} = \frac{1}{3} a_\kappa^{\text{inc}}$: #0.0, ..., $\varepsilon^{(L)}$, #1, ..., $|U(\kappa; z)|$, #2, ..., $|U(2\kappa; z)|$, #3, ..., $|U(3\kappa; z)|$, $\#\, n.1$, ..., $\mathfrak{Re}(\varepsilon_{n\kappa})$, $\#\, n.2$, ..., $\mathfrak{Im}(\varepsilon_{n\kappa})$.

$z \in [-2\pi\delta, 2\pi\delta]$), see Figures 9(b), (d), (f). For given amplitudes a_κ^{inc} and $a_{2\kappa}^{\text{inc}}$, the graph of $\mathfrak{Im}(\varepsilon_{n\kappa}[a_\kappa^{\text{inc}}, a_{2\kappa}^{\text{inc}}, z])$ characterises the *loss of energy* in the nonlinear layer at the excitation frequencies $n\kappa$, $n = 1, 2$, caused by the *generation* of the electromagnetic field of the third harmonic. Such a situation arises because of the right-hand side of (7) at the triple frequency and the generation which is evoked by the right-hand side of (7) at the basic frequency. From Figures 9(b), (d), (f) we see that small values of a_κ^{inc} and $a_{2\kappa}^{\text{inc}}$ induce a small amplitude of the function $\mathfrak{Im}(\varepsilon_{n\kappa})$, i.e., $|\mathfrak{Im}(\varepsilon_{n\kappa})| \approx 0$. The increase of a_κ^{inc}

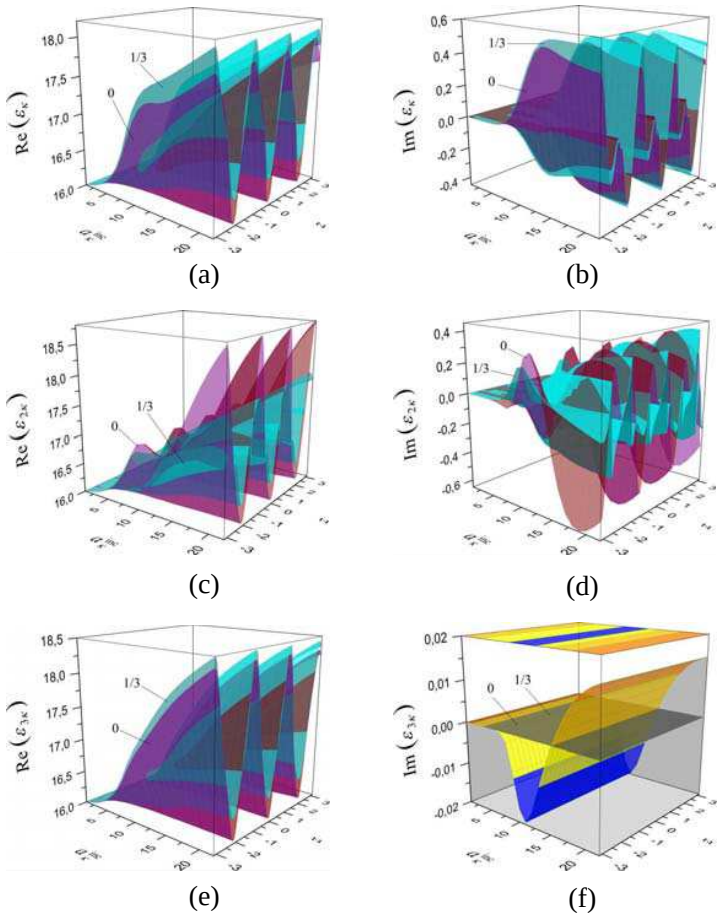

Figure 9. Graphs characterising the nonlinear dielectric permittivity in dependence on $[a_\kappa^{\text{inc}}, a_{2\kappa}^{\text{inc}}, z]$ for $\varphi_\kappa = 60°$ and $a_{2\kappa}^{\text{inc}} = \frac{1}{3} a_\kappa^{\text{inc}}$: (a) $\mathfrak{Re}(\varepsilon_\kappa)$, (b) $\mathfrak{Im}(\varepsilon_\kappa)$, (c) $\mathfrak{Re}(\varepsilon_{2\kappa})$, (d) $\mathfrak{Im}(\varepsilon_{2\kappa})$, (e) $\mathfrak{Re}(\varepsilon_{3\kappa})$, (f) $\mathfrak{Im}(\varepsilon_{3\kappa})$.

corresponds to a strong incident field and leads to the generation of a third harmonic field $U(3\kappa; z)$, and the increase of $a_{2\kappa}^{\text{inc}}$ changes the behaviour of $\varepsilon_{n\kappa}$ (compare the surface #0 with the surfaces #1/3 and #2/3 in Figure 9. Figures 9(b), (d), (f) show the dynamical behaviour of $\mathfrak{Im}(\varepsilon_{n\kappa})$. It can be seen that $\mathfrak{Im}(\varepsilon_{3\kappa}) = 0$, whereas at the same time the values of $\mathfrak{Im}(\varepsilon_{n\kappa})$, $n = 1, 2$, may be *positive or negative* along the height of the nonlinear layer, i.e., in the interval $z \in [-2\pi\delta, 2\pi\delta]$, see (18). The zero values of $\mathfrak{Im}(\varepsilon_{n\kappa})$, $n = 1, 2$, are determined by the phase relations between the scattered and the generated fields in the nonlinear layer, namely at the basic frequency κ by the phase relation between $U(\kappa; z)$, $U(3\kappa; z)$, and at the double frequency 2κ by the phases of $\{U(n\kappa; z)\}_{n=1,2,3}$, see (18):

$$\begin{aligned}
&\delta_{n1}\left[-3\arg(U(\kappa; z)) + \arg(U(3\kappa; z))\right] \\
&+\delta_{n2}\left[-2\arg(U(2\kappa; z)) + \arg(U(\kappa; z)) + \arg(U(3\kappa; z))\right] = p\pi, \\
&p = 0, \pm 1, \ldots, \quad n = 1, 2.
\end{aligned}$$

As in the previous subsection we see that the behaviour of both the quantities $\mathfrak{Re}(\varepsilon_{n\kappa})$ and $\mathfrak{Im}(\varepsilon_{n\kappa})$ (see (19)) plays an essential role in the process of third harmonic generation.

We mention that the impact of a strong electromagnetic field with an amplitude a_{κ}^{inc} even in the absence of a weak field $a_{2\kappa}^{\text{inc}} = 0$ (where $U(2\kappa; z) = 0$) induces a nontrivial component of the nonlinear dielectric permittivity at the frequency 2κ. Figure 9(c) shows that the existence of nontrivial values $\mathfrak{Re}(\varepsilon_{2\kappa}) \neq \mathfrak{Re}(\varepsilon^{(L)})$ and $\mathfrak{Im}(\varepsilon_{2\kappa}) \neq 0$ is caused by the amplitude and phase characteristics of the fields $U(\kappa; z)$ and $U(3\kappa; z)$. Moreover, the nonlinear component of the dielectric permittivity, which is responsible for the variation of $\mathfrak{Re}(\varepsilon_{n\kappa} - \varepsilon_{3\kappa})$ and $\mathfrak{Im}(\varepsilon_{n\kappa})$, does not depend on the absolute value of the amplitude of the field at the double frequency $|U(2\kappa; z)|$, see (19) and (18). Thus, even a weak field includes a mechanism for the redistribution of the energy of the incident wave packet which is consumed for the scattering process and the generation of waves, cf. the dynamics of the surfaces #0 with #1/3 in Figure 9.

The scattering and generation properties of the nonlinear structure are presented in Figures 10&11. Figure 10 shows the same dependencies as in Figures 11(a), (b) but with the additional parameter $a_{2\kappa}^{\text{inc}}$ so that it is possible to track the dynamics of the scattering, generation and energy characteristics of the nonlinear layer under the influence of an incident wave package consisting of a strong and a weak magnetic field with amplitudes a_{κ}^{inc} and $a_{2\kappa}^{\text{inc}}$, resp. The top left diagram in Figure 11 shows the dynamics of the scattering ($R_{\kappa}[\varphi_{\kappa}, a_{\kappa}^{\text{inc}}, a_{2\kappa}^{\text{inc}}]$, $T_{\kappa}[\varphi_{\kappa}, a_{\kappa}^{\text{inc}}, a_{2\kappa}^{\text{inc}}]$, $R_{2\kappa}[\varphi_{\kappa}, a_{\kappa}^{\text{inc}}, a_{2\kappa}^{\text{inc}}]$, $T_{2\kappa}[\varphi_{\kappa}, a_{\kappa}^{\text{inc}}, a_{2\kappa}^{\text{inc}}]$) and generation ($R_{3\kappa}[\varphi_{\kappa}, a_{\kappa}^{\text{inc}}, a_{2\kappa}^{\text{inc}}]$, $T_{3\kappa}[\varphi_{\kappa}, a_{\kappa}^{\text{inc}}, a_{2\kappa}^{\text{inc}}]$) properties of the structure as well

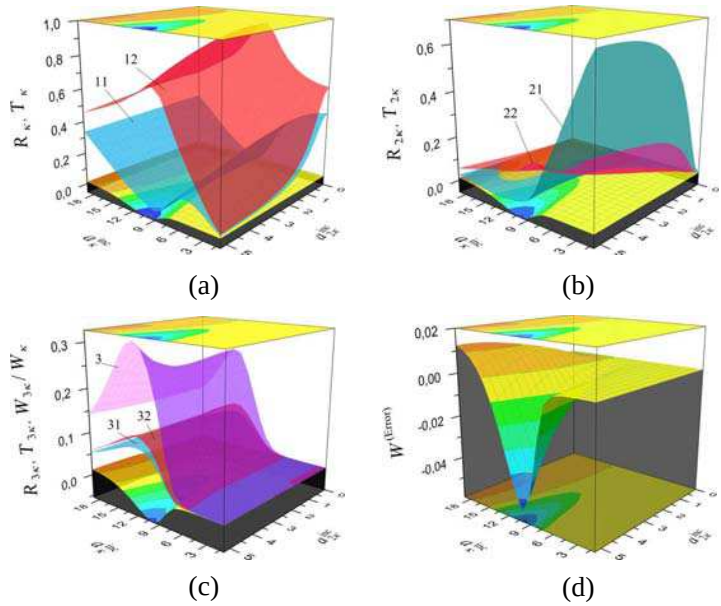

Figure 10. The scattering and generation properties of the nonlinear structure in dependence on $\left[\varphi_\kappa, a_\kappa^{\rm inc}, a_{2\kappa}^{\rm inc}\right]$ for $\varphi_\kappa = 60°$: (a) R_κ, T_κ (#11, #12), (b) $R_{2\kappa}$, $T_{2\kappa}$ (#21, #22), (c) $W_{3\kappa}/W_\kappa$, $R_{3\kappa}$, $T_{3\kappa}$ (#3, #31, #32), (d) $W^{(\rm Error)}$.

as the graph of $W_{3\kappa}[\varphi_\kappa, a_\kappa^{\rm inc}, a_{2\kappa}^{\rm inc}]/W_\kappa[\varphi_\kappa, a_\kappa^{\rm inc}, a_{2\kappa}^{\rm inc}]$ (see Figure 7(a)) for $\varphi_\kappa = 60°$ and $a_\kappa^{\rm inc} = 9.93$.

In the resonant range of wave scattering and generation frequencies, i.e., $\kappa^{\rm scat} := \kappa^{\rm inc} = \kappa$ and $\kappa^{\rm gen} = 3\kappa$, resp., the dynamical behaviour of the characteristic quantities depicted in Figures 10&11 has the following causes. The scattering and generation frequencies are close to the corresponding eigen-frequencies of the linear ($\alpha = 0$) and linearised nonlinear ($\alpha \neq 0$) spectral problems. Furthermore, the distance between the corresponding eigen-frequencies of the spectral problems with $\alpha = 0$ and $\alpha \neq 0$ is small. The graphs of the eigen-fields corresponding to the branches of the considered eigen-frequencies are shown in Figures 11(e), (f).

The second row in Figure 11 depicts the Q-factors Q_{κ_1}, Q_{κ_3} (see (20)) and the quantities $Q_{\kappa_1}(a_{n\kappa}^{\rm inc})/Q_{\kappa_3}(a_{n\kappa}^{\rm inc})$, $\frac{1}{3}\mathfrak{Im}[\kappa_3(a_{n\kappa}^{\rm inc})]/\mathfrak{Im}[\kappa_1(a_{n\kappa}^{\rm inc})]$. We see that the increase in the amplitude of the incident field leads to an increase in the Q-factor of the triple frequency, whereas in the behaviour of the Q-factor of the basic frequency a local minimum is observed, see Figure 11(c). The decrease of Q_{κ_1} at the left-hand side of its local minimum can be correlated with the energy spent on

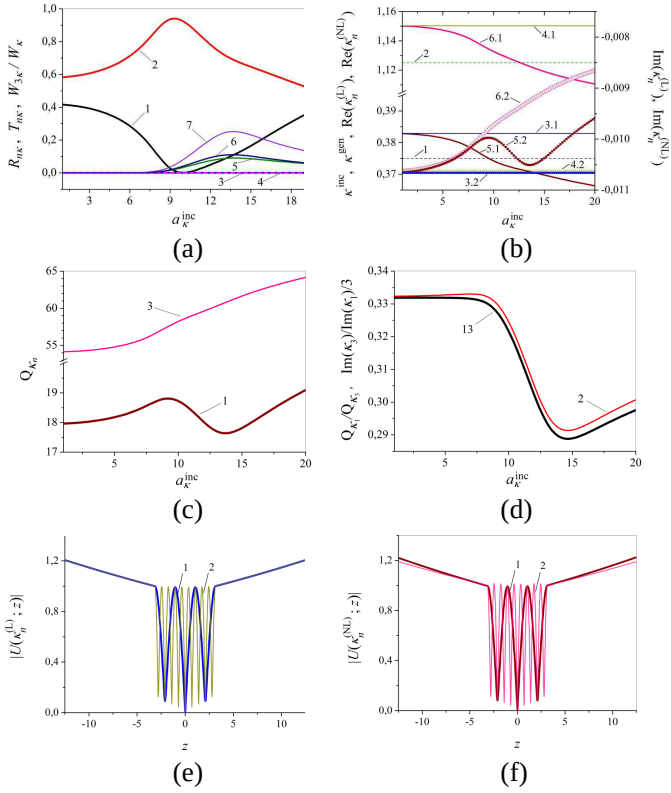

Figure 11. (a) The curves R_κ (#1), T_κ (#2), $R_{2\kappa}$ (#3), $T_{2\kappa}$ (#4), $R_{3\kappa}$ (#5), $T_{3\kappa}$ (#6), $W_{3\kappa}/W_\kappa$ (#7) for $\varphi_\kappa = 60°$, (b) the curves $\kappa := \kappa^{\text{inc}} := 0.375$ (#1), $3\kappa = \kappa^{\text{gen}} = 3\kappa^{\text{inc}} = 1.125$ (#2), the complex eigen-frequencies $\mathfrak{Re}(\kappa_1^{(L)})$ (#3.1), $\mathfrak{Im}(\kappa_1^{(L)})$ (#3.2), $\mathfrak{Re}(\kappa_3^{(L)})$ (#4.1), $\mathfrak{Im}(\kappa_3^{(L)})$ (#4.2) of the linear problem ($\alpha = 0$) and $\mathfrak{Re}(\kappa_1^{(NL)})$ (#5.1), $\mathfrak{Im}(\kappa_1^{(NL)})$ (#5.2), $\mathfrak{Re}(\kappa_3^{(NL)})$ (#6.1), $\mathfrak{Im}(\kappa_3^{(NL)})$ (#6.2) of the linearised nonlinear problem ($\alpha = +0.01$) for $\varphi_\kappa = 60°$; the Q-factors of eigenoscillations of the spectral problem at $\alpha = +0.01$, $\kappa^{\text{inc}} = 0.375$, $\varphi_\kappa = 60°$, $\kappa_n = \kappa_n^{(NL)}$: (c) Q_{κ_1} (#1) and Q_{κ_3} (#3), $Q_{\kappa_1}/Q_{\kappa_3}$ (#13) and (d) $\frac{1}{3}\mathfrak{Im}(\kappa_3)/\mathfrak{Im}(\kappa_1)$ (#2); the graphs of the eigen-fields of the layer for $\varphi_\kappa = 60°$, $a_\kappa^{\text{inc}} = 14$: (e) the linear problem ($\alpha = 0$): $|U(\kappa_1^{(L)}; z)|$ with $\kappa_1^{(L)} = 0.3829155 - i\,0.01066148$ (#1), $|U(\kappa_3^{(L)}; z)|$ with $\kappa_3^{(L)} = 1.150293 - i\,0.01062912$ (#2), (f) the linearised nonlinear problem ($\alpha = +0.01$): $|U(\kappa_1^{(NL)}; z)|$ with $\kappa_1^{(NL)} = 0.3705110 - i\,0.01049613$ (#1), $|U(\kappa_3^{(NL)}; z)|$ with $\kappa_3^{(NL)} = 1.121473 - i\,0.009194824$ (#2).

the generation of the third harmonic. The reduction of Q_{κ_1} starts in the region of canalisation of energy (see #1, where Figure 11(a)). The maximal generation (see #7 in Figure 11(a)) is achieved at the minimum of Q_{κ_1} (see #1 in Figure 11(c) or #13 in Figure 11(d)). Note that in our case study we observe that $Q_{\kappa_1}/Q_{\kappa_3} \approx \frac{1}{3}\Im\mathfrak{m}(\kappa_3)/\Im\mathfrak{m}(\kappa_1)$, see #13 and #2 in Figure 11(d).

Figure 11(b) illustrates the dispersion characteristics of the linear ($\alpha = 0$) and the linearised nonlinear ($\alpha = +0.01$) layer $\varepsilon_{n\kappa} = \varepsilon^{(L)} + \varepsilon^{(NL}_{n\kappa}$, $n = 1, 2, 3$. The nonlinear components of the permittivity at the scattering (excitation) frequencies $\kappa^{\rm scat} := \kappa^{\rm inc} = \kappa$ and the generation frequencies $\kappa^{\rm gen} := 3\kappa$ depend on the amplitude $a^{\rm inc}_{\kappa}$ and the angle of incidence φ_κ of the incident field. This is reflected in the dynamics of the behaviour of the complex-valued eigen-frequencies of the linear and the linearised nonlinear layer.

We start the analysis of the results of our calculations with the comparison of the dispersion relations given by the branches of the eigen-frequencies (curves #3.1, #3.2 and #5.1, #5.2) near the scattering frequency (curve #1, corresponding to the excitation frequency) and (curves #4.1, #4.2, #6.1, #6.2) near the oscillation frequency (line #2) in the situations presented in Figure 11(b). The graph #5.1 lies below the graph #3.1 and the graph #6.1 below the graph #4.1. That is, canalising properties (properties of transparency) of the nonlinear layer occur if $\alpha > 0$. This case is characterised by the increase of the angle of transparency of the nonlinear structure at the excitation frequency with an increasing amplitude of the incident field. The analysis of the eigen-modes of Figure 11(b) allows us to explain the mechanisms of the canalisation phenomena (transparency) (see Figure 11(a) (graph #1)) and wave generation (see Figure 11(a) (graphs #5, #6)).

Comparing the results shown in Figure 11(a) and Figure 11(b) we note the following. The intersection of the curves #1 and #5.1 in Figure 11(b) defines certain parameters, in the neighborhood of which the canalisation effect (transparency) of the nonlinear structure can be observed in Figure 11(a). For example, in Figure 11(b) the curves #1 and #5.1 intersect at $a^{\rm inc}_{\kappa} = 9.5$, also here the curve #5.2 achieves a local maximum. Near this value, we see the phenomenon of canalisation (transparency) of the layer in Figure 11(a). At the point of intersection of the curves #2 and #6.1, the graph #5.2 starts to decrease monotonically in some interval. The intersection of the curves #2 and #6.1 defines the parameter $a^{\rm inc}_{\kappa} = 12.6$, which falls into the range [9.5, 13.6] of values of the amplitudes at which the curve #5.2 is monotonically decreasing. This leads to a shift in the imaginary part of the eigen-frequency of the scattering structure

(graph #5.2) with respect to the eigen-frequency of the generating structure (graph #6.2). The magnitude of the shift depends on the distance between the curves of #6.2 and #5.2 at the given value a_κ^{inc}. The maximal distance between the graphs #6.2 and #5.2 is achieved at the local minimum of the graph #5.2 at $a_\kappa^{\text{inc}} = 13.6$. Right from this point, i.e., with an increasing amplitude a_κ^{inc}, the distance between the graphs #6.2 and #5.2 shows no significant change. The maximum value of the generation is achieved at an amplitude close to the intersection of curves #2 and #6.1, but shifted to the point of the local minimum of the curve #5.2, see $R_{3\kappa}$, $T_{3\kappa}$, $W_{3\kappa}/W_\kappa$ in Figure 11(a) and Figure 7(b).

Figures 11(e), (f) present the characteristic distribution of the eigen-fields corresponding to the branches of the eigen-frequencies under consideration. The graphs of the eigen-fields of type $H_{0,0,4}$ are labeled by #1, the graphs of the eigen-fields of type $H_{0,0,10}$ by #2.

The numerical results presented in this paper were obtained using an approach based on the description of the wave scattering and generation processes in a nonlinear, cubically polarisable layer by a system of nonlinear integral Equation (11), and of the corresponding spectral problems by the nontrivial solutions of (14). We have considered an excitation of the nonlinear layer defined by the condition (15). For this case we passed from (11) to (12) and from (13) to (14) by the help of Simpson's quadrature rule. The numerical solution of (12) was obtained using the self-consistent iterative algorithm ([5, 6]). The problem (14) was solved by means of Newton's method. In the investigated range of parameters, the dimension of the resulting systems of algebraic equations was $N = 301$, and the relative error of calculations did not exceed $\xi = 10^{-7}$.

5. CONCLUSION

We presented results of a computational analysis based on a mathematical model of resonance scattering and generation of waves on an isotropic nonmagnetic nonlinear layered dielectric structure excited by a packet of plane waves in a self-consistent formulation, where the analysis is performed in the domain of resonance frequencies [2, 5, 6]. Here, both the radio [9] and optical [12] frequency ranges are of interest. The wave packets consist of both strong electromagnetic fields at the excitation frequency of the nonlinear structure (leading to the generation of waves) and of weak fields at the multiple frequencies (which do not lead to the generation of harmonics but influence on the process of scattering and generation of waves by the nonlinear structure). The model reduces to a system of nonlinear boundary-value problems of Sturm-Liouville type or, equivalently, to a system of

nonlinear integral equations. The solution of these nonlinear problems was obtained rigorously in a self-consistent formulation and without using approximations of the given field, slowly varying amplitudes etc..

The approximate solution of the nonlinear problems was obtained by means of solutions of linear problems with an induced nonlinear dielectric permeability. The analytical continuation of these linear problems into the region of complex values of the frequency parameter allowed us to switch to the analysis of spectral problems. In the frequency domain, the resonant scattering and generation properties of nonlinear structures are determined by the proximity of the excitation frequencies of the nonlinear structures to the complex eigen-frequencies of the corresponding homogeneous linear spectral problems with the induced nonlinear dielectric permeability of the medium.

We presented a collection of numerical results that describe interesting properties of the nonlinear permittivities of the layers as well as their scattering and generation characteristics. In particular, for a nonlinear single-layered structure with decanalising properties, the effect of type conversion of generated oscillations was observed.

We were able to show the characteristic dynamical behaviour of the relative Q-factor of the eigenmodes and the energy of higher harmonics generated by canalising as well as decanalising nonlinear layers. For an increasing amplitude of the exciting field, an increase of the generated energy in the higher harmonics is accompanied by a monotonic decrease of the relative Q-factor of the eigenoscillations.

The results demonstrate the possibility to control the scattering and generating properties of a nonlinear structure via the intensities of its excitation fields. They also indicate a possibility of designing a frequency multiplier and other electrodynamical devices containing nonlinear dielectrics with controllable permittivity.

ACKNOWLEDGMENT

This work was partially supported by the Visby Program of the Swedish Institute and by the joint Russian-Ukrainian RFBR-NASU grant No. 12.02.90425-2012.

REFERENCES

1. Agranovich, V. and V. Ginzburg, *Spatial Dispersion in Crystal Optics and the Theory of Excitons,* Interscience, London, 1966.
2. Angermann, L., Y. V. Shestopalov, and V. V. Yatsyk, "Modeling and analysis of wave packet scattering and generation for a nonlinear layered structure," *Multiphysics Modeling in Microwave Power Engineering*, 21–26, E. M. Kiley and V. V. Yakovlev (eds.),

University of Bayreuth, Germany, 2012; *14th Seminar Computer Modeling in Microwave Engineering and Applications*, Bayreuth, Mar. 5–6, 2012.

3. Angermann, L. and V. V. Yatsyk, "Numerical simulation of the diffraction of weak electromagnetic waves by a Kerr-type nonlinear dielectric layer," *Int. J. Electromagnetic Waves and Electronic Systems*, Vol. 13, No. 12, 15–30, 2008.
4. Angermann, L. and V. V. Yatsyk, "Mathematical models of the analysis of processes of resonance scattering and generation of the third harmonic by the diffraction of a plane wave through a layered, cubically polarisable structure," *Int. J. Electromagnetic Waves and Electronic Systems*, Vol. 15, No. 1, 36–49, 2010 (in Russian).
5. Angermann, L. and V. V. Yatsyk, "Generation and resonance scattering of waves on cubically polarisable layered structures," *Numerical Simulations — Applications, Examples and Theory*, 175–212, L. Angermann, Ed., InTech, Rijeka/Vienna, Croatia/Austria, 2011.
6. Angermann, L. and V. V. Yatsyk, "Resonance properties of scattering and generation of waves on cubically polarisable dielectric layers," *Electromagnetic Waves*, 299–340, V. Zhurbenko, Ed., InTech, Rijeka/Vienna, Croatia/Austria, 2011.
7. Angermann, L. and V. V. Yatsyk, "The influence of weak fields at multiple frequencies on the process of resonant scattering and generation of oscillations by nonlinear layered structures," *Physical Bases of Instrumentation*, Vol. 2, No. 1, 48–71, 2013 (in Russian).
8. Angermann, L., V. V. Yatsyk, and M. V. Yatsyk, "Preset field approximation and self-consistent analysis of the scattering and generation of oscillations by a layered structure," *Inverse Problems and Large-Scale Computations Springer Proceedings in Mathematics & Statistics*, Vol. 52, 41–56, L. Beilina and Y. V. Shestopalov, Eds., Springer-Verlag, New York, Heidelberg, Dordrecht, London, 2013.
9. Chernogor, L. F., *Nonlinear Radiophysics*, V. N. Karazin Kharkov National University, Kharkov, 2004.
10. Kleinman, D. A., "Nonlinear dielectric polarization in optical media," *Phys. Rev.*, Vol. 126, No. 6, 1977–1979, 1962.
11. Kravchenko, V. F. and V. V. Yatsyk, "Effects of resonant scattering of waves by layered dielectric structure with Kerr-type nonlinearity," *Int. J. Electromagnetic Waves and Electronic Systems*, Vol. 12, No. 12, 17–40, 2007.

12. Miloslavsky, V. K., *Nonlinear Optics,* V. N. Karazin Kharkov National University, Kharkov, 2008.
13. Schürmann, H. W., V. S. Serov, and Y. V. Shestopalov, "Reflection and transmission of a TE-plane wave at a lossless nonlinear dielectric film," *Physica D*, Vol. 158, 197–215, 2001.
14. Serov, V., H. W. Schürmann, and E. Svetogorova. "Integral equation approach to reflection and transmission of a plane TE-wave at a (linear/nonlinear) dielectric film with spatially varying permittivities," *J. Phys. A: Math. Gen.*, Vol. 37, 3489–3500, 2004.
15. Shestopalov, V. and V. V. Yatsyk, "Spectral theory of a dielectric layer and the Morse critical points of dispersion equations," *Ukrainian J. of Physics*, Vol. 42, No. 7, 861–869, 1997.
16. Shestopalov, V. P. and Y. K. Sirenko, *Dynamical Theory of Gratings,* Naukova Dumka, Kiev, 1989 (in Russian).
17. Shestopalov, Y. V. and V. V. Yatsyk, "Resonance scattering of electromagnetic waves by a Kerr nonlinear dielectric layer," *Radiotekhnika i Elektronika (J. of Communications Technology and Electronics)*, Vol. 52, No. 11, 1285–1300, 2007.
18. Shestopalov, Y. V. and V. V. Yatsyk, "Diffraction of electromagnetic waves by a layer filled with a Kerr-type nonlinear medium," *J. of Nonlinear Math. Physics*, Vol. 17, No. 3, 311–335, 2010.
19. Smirnov, Y. G., H. W. Schürmann, and Y. V. Shestopalov, "Propagation of TE-waves in cylindrical nonlinear dielectric waveguides," *Physical Review E*, Vol. 71, 0166141-1–166141-10, 2005.
20. Vaĭnshteĭn, L. A., *Electromagnetic Waves,* Radio i Svyas, Moscow, 1988 (in Russian).
21. Vinogradova, M. B., O. V. Rudenko, and A. P. Sukhorukov, *Wave Theory*, Nauka, Moscow, 1990.
22. Yatsyk, V. V., "A constructive approach to construction of local equations of irregular dispersion and evolution of fields in a quasi-homogeneous electrodynamic structure," *Usp. Sovr. Radioelektroniki*, Vol. 10, 27–44, 2000; Translated in: *Telecommunications and Radio Engineering,* Vol. 56, Nos. 8–9, 89–113, 2001.
23. Yatsyk, V. V., "Diffraction by a layer and layered structure with positive and negative susceptibilities of Kerr-nonlinear media," *Usp. Sovr. Radioelektroniki*, Vol. 8, 68–80, 2006.
24. Yatsyk, V. V., "About a problem of diffraction on transverse non-homogeneous dielectric layer of Kerr-like nonlinearity," *Int. J. Electromagnetic Waves and Electronic Systems*, Vol. 12, No. 1, 59–69, 2007.